Diffusion-Induced Nonuniformity of Photoinitiation in a Photobleaching Medium

Guillermo Terrones*

Applied Physics Division, Los Alamos National Laboratory, Los Alamos, New Mexico 87545

Arne J. Pearlstein*

Department of Mechanical and Industrial Engineering, University of Illinois at Urbana-Champaign, 1206 West Green Street, Urbana, Illinois 61801

Received August 29, 2003; Revised Manuscript Received November 3, 2003

ABSTRACT: Absorption of incident light in photopolymerizations gives rise to instantaneous distributions of initiator concentration and initiation rate that are nonuniform along the beam path. Absent diffusion, however, the time-integrated production of primary radicals is uniform if the initial initiator concentration is uniform and all initiator is consumed, since each initiator molecule is photolyzed in place. Here, we consider the effects of diffusion of a photobleaching initiator for finite values of the ratio of the diffusive time scale l^2/D to the reaction time scale $1/(\phi I_o \alpha_A)$, where l and I_o are the layer thickness and incident light intensity at the optical entrance, and D and α_A are the diffusion coefficient and molar absorption coefficient of photoinitiator, respectively, whose quantum yield of consumption is ϕ. Compared to the limiting case in which diffusion is negligible, diffusion has the effect of shifting the instantaneous initiation rate profiles forward in the layer, where initiator is relatively depleted. On the other hand, for any nonzero initial absorbance, the overall (i.e., time-integrated) consumption of initiator becomes more *nonuniform* as the ratio of the rates of diffusion and reaction, expressed in the dimensionless ratio $\delta = D/(l^2\phi I_o \alpha_A)$, increases. When diffusion is fast (large δ), the front-to-back difference in the time-integrated primary radical production varies quadratically with the initial concentration of initiator. Implications of the results for conversion of monomer and for chain-length distributions are discussed.

Introduction

Photopolymerization in strongly absorbing media occurs in a number of applications, including photolithography, fabrication of dental prostheses and orthopedic components, and production of paints, adhesives, and other coatings.[1,2] An essential characteristic of any photochemical reaction is inherent spatial nonuniformity of the reaction rate, due to the dependence of local rates on local light intensity. Since the light intensity $I(x,t)$ decreases along the beam path according to

$$\frac{\partial I(x,t)}{\partial x} = -\left[\sum_{i=1}^{N} \alpha_i C_i(x,t)\right] I(x,t) \qquad (1)$$

reduction of the local value of the optical density, i.e., the first factor in (1), will have the effect of increasing the light intensity at each position "downbeam", where α_i and C_i are the absorption coefficient and concentration of the ith absorbing species, of which there are $N \geq 1$. (The definitions and units for the symbols used throughout the paper are given in Table 1.) In strongly absorbing media, attenuation is sufficiently strong that essentially all actinic radiation is absorbed in a very thin layer. Since the rates of primary photochemical processes are generally proportional to the product of concentration and local light intensity, attenuation necessarily gives rise to spatial and temporal variation in the local rates of photochemical processes and subsequent kinetic steps. The nonuniformity of the rate of reaction in turn results in nonuniform concentration profiles of the light-absorbing reactant(s), as well as spatially varying product distributions. We have recently discussed spatiotemporal variation of the initiation rate in a photobleaching medium,[1] as well as its effects on the rate of monomer conversion[2] and on chain-length distributions (CLDs)[3] in ensuing free-radical photopolymerization.

Diffusion is potentially important in systems with large concentration gradients. Since the characteristic time for diffusion is given by $t_{diff} = l^2/D$, where l is a characteristic length over which concentration variation is significant and D is the diffusion coefficient of the diffusing species, we can state definitively that diffusion will not be important if all time scales (e.g., overall processing time and temporal period of time-periodic illumination[4]) are much shorter than t_{diff}. We note that, at very high optical densities, the concentration variation, absent diffusion, is confined to a very thin region into which light can penetrate, so that l can be substantially smaller than the layer thickness.

One application in which diffusion can be important is layered microstereophotolithographic fabrication of three-dimensional structures by photopolymerization initiated by single-photon absorption by an initiator.[5−7] In that application, high optical density is essential in confining reaction to a thin surface layer. Photobleaching of the initiator results in loss of "vertical resolution". Diffusion will be significant in such a system if the dimensionless quantity Dt/l^2 is on the order of 1 or more. For a typical length scale of interest in this application ($\sim$30 μm), diffusion will be significant if $Dt > 9 \times 10^{-6}$ cm^2. For a diffusion coefficient of 10^{-5} cm^2 s^{-1}, appropriate to the low-viscosity resins used[7] to avoid damage to the structure during addition of resin for each additional layer, we see that diffusion will be important for photo-

* To whom correspondence should be addressed.

10.1021/ma030451e CCC: $27.50
Published on Web 01/27/2004

Table 1

symbol	quantity	definition	units
C_i	concentration of species i		M
$C_{i,0}$	initial concentration of species i		M
D	diffusion coefficient of initiator		$m^2\ s^{-1}$
f	number of primary radicals created per photoinitiator molecule consumed		
I	light intensity		einsteins $m^{-2}\ s^{-1}$
I_o	incident light intensity		einsteins $m^{-2}\ s^{-1}$
k_p	propagation rate constant		$M^{-1}\ s^{-1}$
k_t	termination rate constant		$M^{-1}\ s^{-1}$
l	characteristic length		m
L	layer depth		m
R_i	dimensional initiation rate	given by (14)	$M\ s^{-1}$
$\tilde{R}_i$	dimensionless initiation rate	$R_i/(\phi I_o \alpha_A C_{A,0})$	
S	dimensionless initiator concentration	$C_A/C_{A,0}$	
S_0	dimensionless initiator concentration absent diffusion		
$\bar{S}$	layer-averaged dimensionless initiator concentration		
t	dimensional time		s
x	dimensional coordinate		m
z	dimensionless coordinate	x/L	
α_i	absorption coefficient of species i		$M^{-1}\ m^{-1}$
β	dimensionless "kinetic" parameter	$k_p[fC_{A,0}/(\phi\alpha_A I_o k_t)]^{1/2}$	
γ	initial absorbance	$\alpha_A C_{A,0} L$	
δ	dimensionless ratio of diffusion and reaction rates	$D/(l^2\phi I_o \alpha_A)$	
Θ	dimensionless time-integrated radical production	given by (15)	
$\Delta\Theta$	front-to back difference in dimensionless time-integrated radical production	given by (17)	
τ	dimensionless time	$\phi I_o \alpha_A t$	
ϕ	quantum yield of initiator consumption		
Ξ	dimensionless concentration difference, predicted with and without diffusion	$S - S_0$	

polymerization times on the order of at least 1 s. Exposure times greater than 1 s have been used in microstereophotolithographic polymerization experiments by Kodama,[8] Brulle et al.,[9] and Maffezzoli and Terzi.[10] While the models proposed and used by previous authors[11,12] approximately account for nonuniformity associated with attenuation of incident light, focusing on the lateral nonuniformity in depth of penetration and cure due to the Gaussian variation in the incident radiation intensity, as well as temperature variations due to nonuniform absorption and reaction, none account for diffusion parallel or perpendicular to the direction of light propagation. Using the same $Dt/l^2 > 1$ criterion, diffusion can be expected to affect the photoinitiator profile in the 15 s photopolymerization of adhesion-inhibiting hydrogels for postsurgical wound treatment reported by Hill-West et al.,[13] provided that $D > 9 \times 10^{-7}\ cm^2\ s^{-1}$.

In general, concentration profiles can be expected to become more nonuniform as the optical density increases, corresponding to decreased optical penetration depth. More precisely, the nonuniformity of the initiator profile at a given degree of initiator consumption is expected to increase as the absorbance (product of optical density and layer thickness) increases. Absent diffusion, we have shown[1] that the photoinitiator profile at a given degree of consumption depends only on the initial absorbance, and that the characteristic length over which this concentration variation occurs will decrease as the optical density increases.

Diffusion and convective mixing can smooth out concentration profiles that result from nonuniform light absorption and reaction. Mixing[14] can result from molecular diffusion in a stagnant medium, or from fluid motion driven by a moving boundary, buoyancy (as discussed by Brulle et al.[9] in the context of stereophotolithography, when density depends on temperature), or variation of surface tension with temperature (or composition). In this paper we focus on the case of strictly diffusive mixing, as occurs in systems with small values of the Peclet number $Pe = Ul/D$, where U is the characteristic fluid velocity. This is the regime of interest in semiconductor photomask development and other thin-layer photopolymerization applications where the length scale l is small enough that bulk fluid motion is likely to be unimportant.

The importance of diffusion in photopolymerizations has been reviewed by Krongauz.[15] Although that review thoroughly discusses applications in which monomer diffusion is important, no reference is made to systems in which photoinitiator diffusion is important, even though (a) nonuniformity of initiator concentration is a major contributor to the nonuniformity of the photoinitiation rate, which is frequently the dominant contributor to nonuniformity in the monomer concentration, and (b) the monomer and photoinitiator typically have molecular weights (and hence diffusion coefficients) on the same order.

To date, most theoretical treatments of photochemical kinetics in high-absorbance systems have neglected diffusion. Exceptions include the work of Hill and coworkers[16−18] and Harano and Smith.[19] More recently, diffusion and spatial variation associated with nonuniform light absorption have been explicitly accounted for by several authors. Terrones and Pearlstein[20] developed and analyzed a model of phenyl azide photolysis and the ensuing chain propagation and termination reactions of the nitrene radicals thus produced, accounting, apparently for the first time, for the effects of diffusion on kinetics in a photobleaching system. In the photopolymerization context, Goodner and Bowman[21] recently presented computations for a model accounting for diffusion of monomer, but not initiator. Their model, which also accounts for heat generation and heat transfer, is restricted to initiators that do not undergo photobleaching. Contemporaneously, Miller et al.[22] considered initiator distribution in a layer in which monomer, polymer, and reaction products resulting from initiator photolysis can also contribute to light absorption. Those authors presented a figure showing photo-

initiator profiles with no diffusion, infinitely fast diffusion (uniform concentration), and a diffusion coefficient of 0.001 $cm^2\ s^{-1}$, each for a single initial initiator concentration (0.0268 M), layer thickness (1 cm), quantum yield (0.2), extinction coefficient (97.7 $M^{-1}\ cm^{-1}$), and light intensity (corresponding to 10 mW mm^{-2} at an unspecified wavelength), at a single time (25 s). The large diffusion coefficient was chosen to provide an upper bound on the magnitude of diffusion effects for the specified values of the other parameters. Miller et al.[22] state that "Diffusion will be more important for photobleaching systems containing high initiator concentrations, which lead to steep concentration gradients and relatively long times for photobleaching." While this conclusion seems correct, the limited results presented provide little insight into how the magnitude of the effects depends on the initiator concentration, layer depth, absorption coefficient, and other parameters.

Here, we extend our recent investigations of the effects of light intensity, initial absorbance, and initiator consumption in systems with photobleaching initiators to account for initiator diffusion. The primary emphasis is on understanding how diffusion increases the nonuniformity of the time-integrated primary radical production rate as a function of layer thickness, diffusion coefficient, initial absorbance of the layer, and other parameters. As in our earlier work absent diffusion, the results are presented in nondimensional form for a wide range of the dimensionless parameters (two in this case), allowing the effects of diffusion on the initiator concentration profiles, the spatiotemporal variation of the initiation rate, and the uniformity of the time-integrated primary radical production to be assessed for essentially the entire range of the five dimensional parameters (initiator concentration, absorption coefficient, diffusion coefficient, layer thickness, and incident intensity) and quantum yield.

As before, we restrict attention to a single-step reaction

$$A \xrightarrow{h\nu} 2R^{\bullet} \tag{2}$$

with first-order kinetics. We further assume that only A absorbs light, and that absorption can be described by a single absorption coefficient, corresponding to absorption either at a single actinic wavelength, or with a constant absorption coefficient over a range of actinic wavelengths. The model is applicable to several situations of practical interest.

First, in photopolymerizations where only the initiator absorbs, the model predicts the local rate of initiator consumption, from which the spatiotemporal variation of the photopolymerization rate can be determined, analogously to the approach demonstrated in our earlier work for the diffusionless case.[2] Detailed understanding of the spatiotemporal variation of the photoinitiation rate is important in understanding depth of cure, residual monomer concentration distributions, and other nonhomogeneous phenomena in photopolymerization. The spatiotemporal variation of the photoinitiation rate is also a critical input to kinetic models predicting the nonuniformity of CLDs.[3]

Second, the governing equations presented and analyzed below are applicable to predicting the effect of diffusion on the concentration variation of any photobleaching species consumed in a single-step process with first-order kinetics due to single-photon photochemical reaction under conditions where light absorption can be modeled using a single absorption coefficient. The approach is also applicable to predicting the concentration distributions of photobleaching photosensitizers used with initiators that do not absorb light directly,[23,24] as well as the profiles of other photobleachable species.

Mathematical Model

Aside from the inclusion of initiator diffusion, the model is identical to that considered in our earlier work,[1] to which the reader is referred for additional details. We consider reaction 2 with quantum yield ϕ in a layer of thickness L subjected to uniform illumination normal to one surface. Transmission and absorption of light by the absorber are assumed to be described by Beer's law, with the intensity at time t and a distance x from the surface at which the light enters the layer (at $x = 0$) being governed by (1), the solution of which is

$$I(x,t) = I_o \exp[-\alpha_A \int_0^x C_A(x',t)\, dx'] \tag{3}$$

where $I(x,t)$ is the light intensity within the medium and I_o is the incident light intensity at the optical entrance. The products and other species are assumed transparent in the wavelength range of interest. The variation of composition along the optical path is then governed by

$$\frac{\partial C_A}{\partial t} = D\frac{\partial^2 C_A}{\partial x^2} - \phi\alpha_A I_o \exp[-\alpha_A \int_0^x C_A(x',t)\, dx']C_A \tag{4}$$

where D is the diffusion coefficient of A. We have assumed that D is constant, and that convective transport is negligible.

We assume that the initiator concentration is initially uniform throughout the layer

$$C_A(x,0) = C_{A,0} \tag{5a}$$

and apply the no-flux condition at the optical entrance and exit (at $x = 0$ and L, respectively)

$$\frac{\partial C_A(0,t)}{\partial x} = \frac{\partial C_A(L,t)}{\partial x} = 0 \tag{5b,c}$$

The number of parameters upon which the solution depends is reduced by nondimensionalizing (3−5), allowing the parameter space to be thoroughly explored with a reasonable amount of computation. We define dimensionless independent and dependent variables $\tau = \phi I_o \alpha_A t$, $z = x/L$, and $S = C_A/C_{A,0}$, along with the dimensionless parameters $\gamma = \alpha_A C_{A,0} L$ and $\delta = D/(L^2 \phi I_o \alpha_A)$. Here, γ is the initial absorbance, and we can think of δ as the dimensionless ratio of the rates of photoinitiator diffusion and consumption. With this nondimensionalization, (4) can be written as

$$\frac{\partial S}{\partial \tau} = \delta\frac{\partial^2 S}{\partial z^2} - \exp[-\gamma \int_0^z S(z',\tau)\, dz']S \tag{6}$$

subject to the initial and boundary conditions

$$S(z,0) = 1 \tag{7a}$$

$$\frac{\partial S(0,\tau)}{\partial z} = \frac{\partial S(1,\tau)}{\partial z} = 0 \tag{7b,c}$$

Equations 6 and 7 constitute an initial-boundary value problem for a nonlinear partial integro−differential equation.

We are aware of no closed-form solution of (6) and (7). Two analytical results will, however, prove useful in assessing the accuracy of the numerical solutions, as well as in understanding the individual and joint effects of diffusion and optical thickness on the evolution of nonuniform concentration profiles.

First, the mean of the dimensionless concentration over the thickness of the layer, given by

$$\bar{S}(\tau) = \int_0^1 S(z,\tau)\, dz \tag{8}$$

satisfies an ordinary differential equation, obtained by integrating (6) over $0 \le z \le 1$, using integration by parts, and invoking (7b) and (7c) to get

$$\frac{d\bar{S}}{d\tau} = -\frac{1}{\gamma}(1 - e^{-\gamma\bar{S}}) \tag{9a}$$

subject to

$$\bar{S}(0) = 1 \tag{9b}$$

The solution of (9a) and (9b) is

$$\bar{S}(\tau) = \frac{1}{\gamma}\ln[1 + (e^{\gamma} - 1)e^{-\tau}] \tag{10}$$

independent of δ (and hence independent of the diffusion coefficient). The extent to which the integral on the right-hand side of (8), of a numerical solution of (6) and (7), departs from the exact result given by (10) provides a measure of the accuracy of the numerical solution. As discussed in the Numerical Approach, departures from (10) were negligible in all cases.

Second, absent diffusion, (6) reduces to a "hyperbolic" integro−partial differential equation

$$\frac{\partial S_0}{\partial \tau} = -\exp[-\gamma\int_0^z S_0(z',\tau)\, dz']S_0 \tag{11}$$

with the initial condition (7a), whose solution[25] can be written as

$$S_0(z,\tau) = [1 + e^{-\gamma z}(e^{\tau} - 1)]^{-1} \tag{12}$$

where S_0 denotes the concentration distribution with no diffusion ($\delta = 0$). Comparison of numerical solutions of (6) and (7) to the exact diffusionless result will provide a clear delineation of the effects of diffusion, with the effects of nonuniform absorption absent diffusion being accounted for by (12).

The dimensionless instantaneous initiation rate is given by

$$\tilde{R}_i(z,\tau) = 2\exp[-\gamma\int_0^z S(z',\tau)\, dz']S(z,\tau) \tag{13}$$

and is related to the dimensional rate

$$R_i(x,t) = 2\phi I_o\alpha_A \exp[-\alpha_A\int_0^x C_A(x',t)\, dx']C_A(x,t) \tag{14}$$

by $R_i(x,t) = \phi I_o\alpha_A C_{A,0}\tilde{R}_i(x/L,\phi I_o\alpha_A t)$. As shown in the Results, comparison of distributions of $\tilde{R}_i$ computed from (6) and (7) to the "diffusionless" ($\delta = 0$) $\tilde{R}_i$ distributions allows for clear assignment of the effects of diffusion and nonuniform absorption in the local instantaneous photoinitiation rate.

We also compute the spatial variation of the dimensionless time-integrated primary radical production

$$\Theta(z;\delta,\gamma) = \int_0^\infty \tilde{R}_i(z,\tau)\, d\tau = 2\int_0^\infty S(z,\tau)\exp[-\gamma\int_0^z S(z',\tau)\, dz']\, d\tau \tag{15}$$

which measures the number of primary radicals produced at each location, integrated over the duration of the process. When there is no diffusion, the number of radicals produced during the entire course of the process is independent of position and initial absorbance, since every initiator molecule gives rise to two radicals *at its initial position*. The computed distributions $\Theta(z;\delta,\gamma)$ are compared to both the fast-diffusion limit

$$\Theta(z;\infty,\gamma) = \frac{2}{\gamma}\int_1^{e^{\gamma}} \frac{\ln x}{x^z(x-1)}\, dx \tag{16}$$

obtained using (10) and (15), for which $S(z,\tau) = \bar{S}(\tau)$, and to the no-diffusion limit, for which $\Theta(z;0,\gamma) = 2$.

Numerical Approach

The initial-boundary value problem (6, 7) was discretized using second-order accurate central-difference and Crank−Nicolson approximations to the spatial and temporal derivatives, respectively, and the trapezoidal rule to approximate the integral.[26] The resulting system of nonlinear transcendental equations at each time step was solved by Newton iteration, with a relative error tolerance of 10^{-7}. Since, at each z, the integral in (6) involves only upbeam values of S, the upper triangular portion of the Jacobian matrix is constant. Accuracy was assessed by halving the time step and spatial grid size. Five hundred grid points were sufficient to ensure an error of less than 0.01% in the front-to-back nonuniformity

$$\Delta\Theta(\delta,\gamma) = \Theta(0;\delta,\gamma) - \Theta(1;\delta,\gamma), \tag{17}$$

which is the primary quantity of interest, except for extreme cases, for which more points were required (e.g., 1500 points for $\gamma = 100$ and $\delta = 10^{-4}$) to achieve the same error control. The uniform time step was reduced and the duration of the temporal integration in (15) was increased until convergence was attained. In all cases for which results are presented below, the magnitude of the absolute difference between the spatially averaged concentration determined numerically and the exact result (10) was less than 10^{-5}.

Results

For several values of the initial absorbance γ and a range of the diffusion/reaction rate ratio δ, we have computed the spatial variation of the dimensionless time-integrated primary radical production $\Theta(z;\delta,\gamma)$. When there is no diffusion, $\Theta(z;0,\gamma) = 2$, as discussed above. As we will see, the effect of diffusion is to shift initiator photolysis toward the optical "front" of the layer, with the effect becoming more important as the initial absorbance γ increases.

We discuss and explain the integrated profiles $\Theta(z;\delta,\gamma)$ in terms of the dimensionless profiles of initiator concentration and instantaneous initiation rate (as functions of $z = x/L$) at fractional initiator consumptions

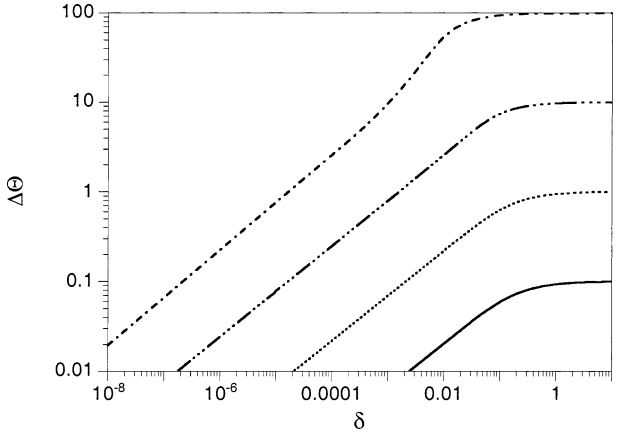

Figure 1. Overall front-to-back variation of time-integrated primary radical production $\Delta\Theta$ as a function of the diffusion/reaction rate ratio δ: —, $\gamma = 0.1$; ···, $\gamma = 1$; −···−, $\gamma = 10$; −·−, $\gamma = 100$.

$1 - \bar{S}$ of 0.1, 0.25, 0.5, 0.75, and 0.9. In each case, the corresponding diffusionless profile (12) is shown for comparison, thus allowing the effects of diffusion to be distinguished from those of attenuation and initiator consumption discussed earlier.[1] We note that (10) and (12) can be combined to give diffusionless profiles in terms of $\bar{S}$

$$S_0(z,\bar{S}) = \frac{1 - e^{-\gamma\bar{S}}}{1 - e^{-\gamma\bar{S}} + e^{\gamma(1-\bar{S}-z)} - e^{-\gamma z}} \qquad (18)$$

so that, for each degree of initiator consumption, the diffusionless profile depends only on γ.

The values of γ and δ for which we present results cover the entire range of behavior, from small γ, for which diffusion is unimportant since the profiles are nearly uniform regardless of δ, to large γ, for which diffusion is important unless δ is very small. The overall front-to-back variation in the time-integrated radical production is bounded above by $\Delta\Theta(\infty,\gamma) = \gamma$, as one can easily show from (16).

The main results of our computations are displayed in Figure 1, where we show how the overall front-to-back nonuniformity $\Delta\Theta$ depends on the initial absorbance γ and diffusion/reaction rate ratio δ.

Figure 1 shows that the high-δ asymptotic value of $\Delta\Theta$ is achieved at progressively smaller values of δ as γ increases, ranging from $\delta \sim 1$ for $\gamma = 0.1$ to $\delta \sim 0.05$ for $\gamma = 100$. This results from the fact that as γ increases, initiator consumption is localized to an increasingly thin layer near the optical entrance, thus reducing the magnitude of the diffusion coefficient required to maintain nearly uniform initiator concentration. For small γ, it can be shown that

$$\Delta\Theta = 2\gamma\delta^{1/2} \tanh \frac{1}{2\delta^{1/2}} + O(\gamma^2) \qquad (19)$$

We note that, for $\gamma \leq 10$, the leading-order term in (19) provides a good approximation over the entire range of δ (error less than 1.1%, 9%, and 25% at $\gamma = 0.1$, 1, and 10, respectively).

We next consider how $\Delta\Theta$ is determined by the spatial profiles $\Theta(z;\delta,\gamma)$, which are in turn related to the dimensionless concentration profiles $S(z,\tau)$ (or $S(z,\bar{S})$ when parametrized by the extent of initiator consumption).

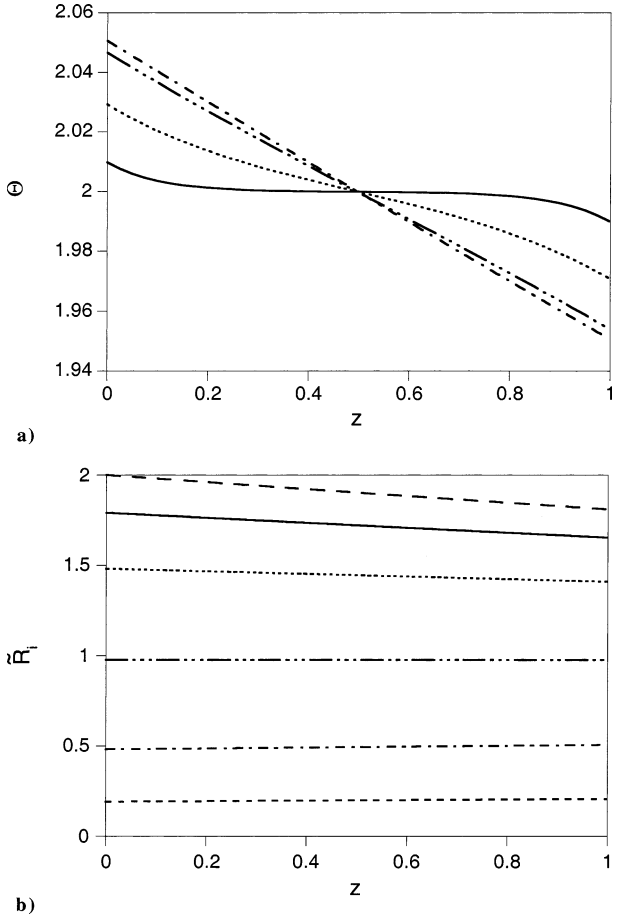

Figure 2. For $\gamma = 0.1$, (a) time-integrated primary radical production Θ as a function of the coordinate $z = x/L$ (—, $\delta = 0.01$; ···, $\delta = 0.1$: −···−, $\delta = 1$; −·−, $\delta = \infty$) and (b) instantaneous initiation rate profiles for $\delta = 0$ as a function of overall consumption of initiator (—, $1 - \bar{S} = 0.1$; ···, $1 - \bar{S} = 0.25$; −···−, $1 - \bar{S} = 0.5$; −·−, $1 - \bar{S} = 0.75$; - - -, $1 - \bar{S} = 0.9$).

$\gamma = 0.1$. For $\gamma = 0.1$, Figure 2a shows that the time-integrated primary radical production Θ is nearly uniform for all δ. At small δ, variation is largely confined to the extreme front and back of the layer. As δ increases, Θ approaches a nearly linear distribution in z. For $\gamma = 0.1$ and $\delta = 0$ (no diffusion), Figure 2b shows the corresponding instantaneous initiation rate profiles for several fractional consumptions of initiator. The departures from uniformity, while small, are greatest at the smallest degrees of initiator consumption, when the overall absorbance is greatest. By the time $1 - \bar{S} = 0.5$, the instantaneous initiation rate at this small initial absorbance is essentially uniform, even absent diffusion. The corresponding concentration profiles (see the Supporting Information) are nearly uniform, a result due to the fact that, for small γ, the first factor in the second term on the right-hand side of (6) is practically constant, thus suppressing the only source of nonuniformity. Since the instantaneous concentration and initiation rate profiles are nearly uniform for $\delta = 0$ (i.e., with no diffusion), it is clear that diffusion will have no significant effect on these profiles for any nonzero δ. Physically, we note that if γ is small, then light absorption and hence the photoinitiator concentration and initiation rate are essentially uniform throughout the layer, regardless of δ.

$\gamma = 1$. For $\gamma = 1$, Figure 3a shows that the dependence of the time-integrated primary radical production dis-

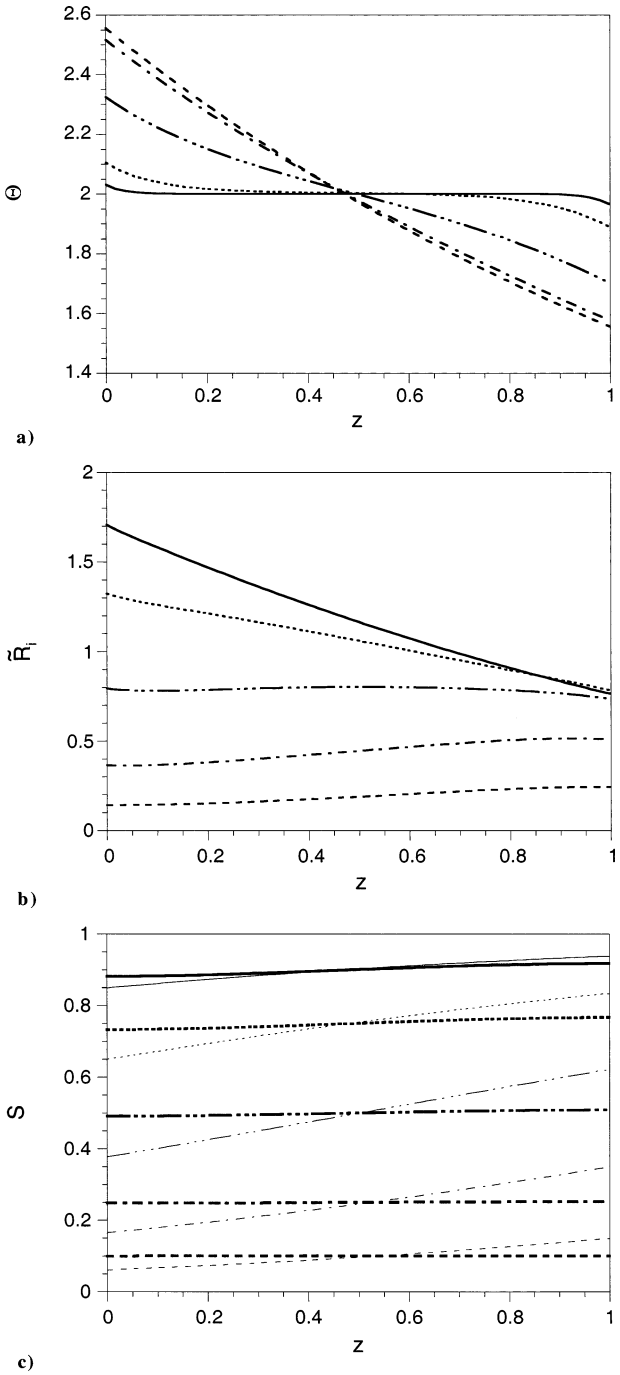

Figure 3. For $\gamma = 1$, (a) time-integrated primary radical production Θ as a function of the coordinate $z = x/L$ (—, $\delta = 10^{-3}$; ···, $\delta = 0.01$; —···—, $\delta = 0.1$; —·—, $\delta = 1$; - - -, $\delta = \infty$) and (b) instantaneous initiation rate profiles for $\delta = 0.01$ and (c) initiator concentration profiles for $\delta = 1$, both as functions of overall consumption of initiator (—, $1 - \bar{S} = 0.1$; ···, $1 - \bar{S} = 0.25$; —···—, $1 - \bar{S} = 0.5$; —·—, $1 - \bar{S} = 0.75$; - - -, $1 - \bar{S} = 0.9$). In (c), thick curves denote results accounting for diffusion, and thin curves denote results neglecting diffusion.

tribution on δ is qualitatively similar to that predicted for $\gamma = 0.1$. The two sets of curves can be made to approximately coincide if scaled according to $[\Theta(z;\delta,\gamma) - 2]/\Delta\Theta(\delta,\gamma)$. As δ increases, the variation in Θ is less confined to the front and back of the layer, with the limiting case of infinitely fast diffusion ($\delta \rightarrow \infty$) showing more curvature for $\gamma = 1$ than for $\gamma = 0.1$, due to greater nonuniformity of absorption. Figure 3b shows profiles of $\tilde{R}_i$ for $\delta = 0.01$. Like those for the diffusionless case,[1] the instantaneous initiation rate profiles for $\delta = 0.01$ decrease monotonically with z for small degrees of consumption, and increase monotonically with z as initiator consumption nears completion. At each degree of initiator consumption, the instantaneous rate near the front of the layer is predicted to be greater for $\delta = 1$ (see the Supporting Information) than for $\delta = 0.01$. The effect is most noticeable for $1 - \bar{S} \geq 0.5$, with the rate decreasing monotonically with z for $\delta = 1$, increasing monotonically with z for $\delta = 0.01$, and being much more uniform for $\delta = 1$ than for $\delta = 0.01$. This shows the effect of diffusion in homogenizing the distribution of initiator. Compared to the results for $\delta = 0.01$, $\tilde{R}_i$ for $\delta = 1$ is larger at $z = 0$ and is smaller at $z = 1$. This result is a simple consequence of the fact that diffusion transports initiator toward the front wall, where, absent diffusion, its concentration would otherwise be lower. Thus, at every degree of initiator consumption, diffusion leads to a monotonic increase in the front-to-back difference in instantaneous initiation rate $\tilde{R}_i(0,\tau) - \tilde{R}_i(1,\tau)$ as δ increases.

Concentration profiles for $\gamma = 1$ and $\delta = 0.01$ and 1 show that, at each degree of initiator consumption, the profile is more uniform (and deviates more from the diffusionless results) for $\delta = 1$ (Figure 3c) than for $\delta = 0.01$ (see the Supporting Information), with the greatest nonuniformity being at the smallest degree of consumption, when the absorbance is highest and light absorption is most nonuniform. Except near $z = 0$ and 1, at which boundary satisfaction of the no-flux conditions (7b) and (7c) requires that the concentration gradient vanish, the concentration profiles vary more linearly with the coordinate z than do the initiation rate profiles for the same values of δ. As discussed earlier,[1] this is a direct consequence of the nonuniform consumption of initiator, in which absorption (and hence consumption) are concentrated near $z = 0$ in the early stages, and near $z = 1$ in the later stages when most of the upbeam initiator has been consumed. For $\gamma = 1$ and $\delta = 0.01$, the concentration and initiation rate profiles are very similar to those for no diffusion, except near $z = 0$ and 1, where diffusion smoothes out the concentration distribution, consistent with the requirement (7b, 7c) that the concentration gradient vanish at the front and back walls, through which no diffusion can occur. Comparison of Figure 3b of ref 1 to Figure 3b in this paper shows that, for $\delta = 1$, the front and back zones, in which diffusion leads to departures from the diffusionless initiation rate profiles, thicken as initiator is consumed. Diffusion leads to significant departures from the diffusionless profiles over a range of spatial locations and fractional consumptions, with noticeable flattening being first apparent near $z = 0$ as early as a fractional consumption of 0.1. By the time the fractional consumption reaches 0.25, the effects of diffusion are apparent in the forward 20% and the rear 20% of the layer. With increasing initiator consumption, the effects of diffusion become significant over a wider range of z. In each case, the difference between the computed profiles and the diffusionless profiles, $\Xi(z,\bar{S}) = S(z,\bar{S}) - S_0(z,\bar{S})$, is nearly antisymmetric about the middle of the layer, $z = 1/2$; i.e., $\Xi(z,\bar{S}) \approx -\Xi(1 - z,\bar{S})$.

$\gamma = 10$. For $\gamma = 10$, Figure 4a shows that the time-integrated primary radical production for each δ is much more nonuniform than for the $\gamma = 1$ cases shown in Figure 3a. Maintenance of a given degree of uniformity in Θ requires smaller values of δ as γ increases, with, for example, $\Delta\Theta(\delta,\gamma) = 0.1$ allowing $\delta = \infty$ at $\gamma = 0.1$,

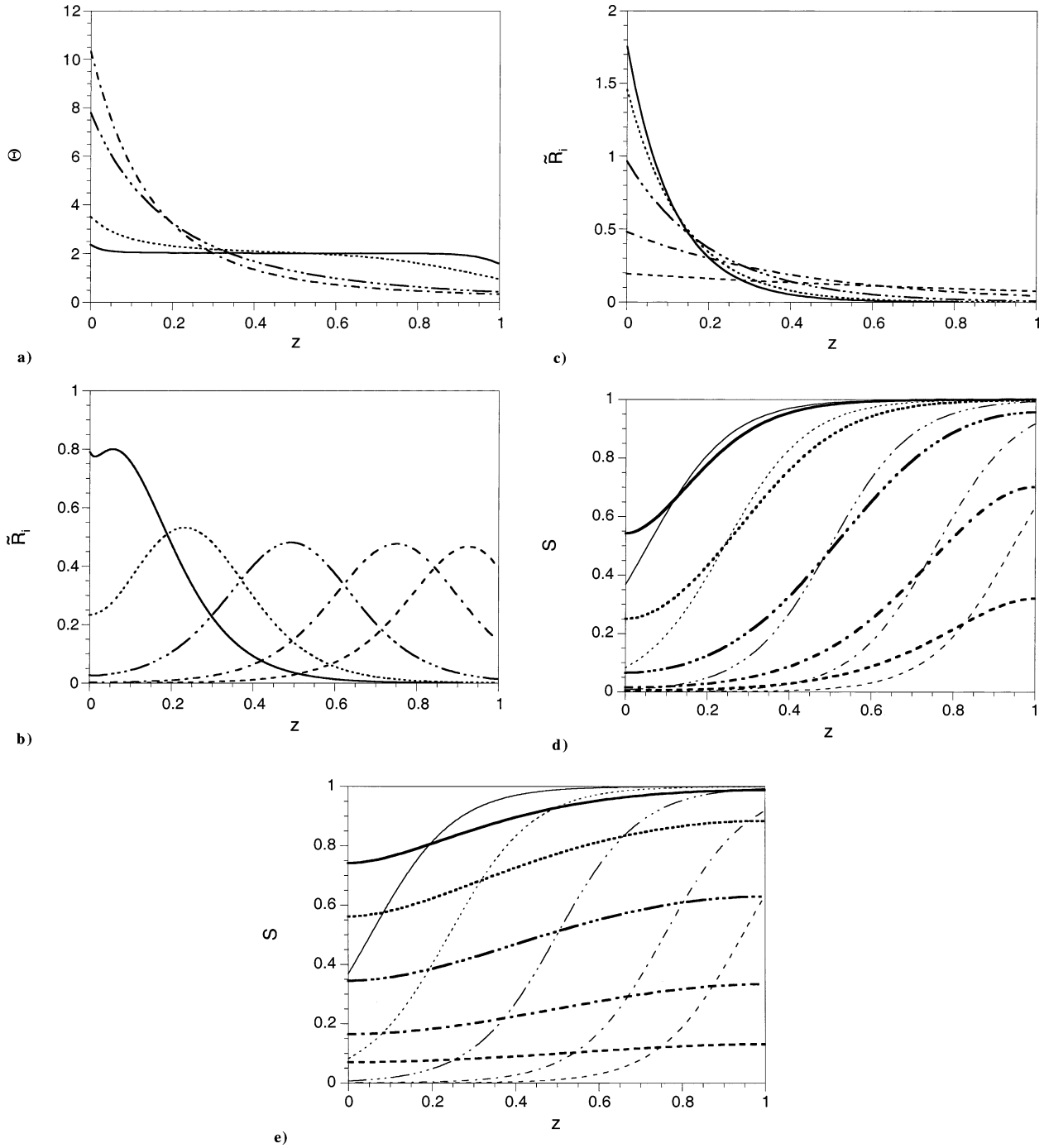

Figure 4. For $\gamma = 10$, (a) time-integrated primary radical production Θ as a function of the coordinate $z = x/L$ (—, $\delta = 10^{-3}$; ···, $\delta = 0.01$: —···—, $\delta = 0.1$; - - -, $\delta = \infty$) and (b) instantaneous initiation rate profiles for $\delta = 10^{-3}$, (c) instantaneous initiation rate profiles for $\delta = 1$, (d) initiator concentration profiles for $\delta = 0.01$, and (e) initiator concentration profiles for $\delta = 0.1$, all as functions of overall consumption of initiator (—, $1 - \bar{S} = 0.1$; ···, $1 - \bar{S} = 0.25$; —···—, $1 - \bar{S} = 0.5$; —·—, $1 - \bar{S} = 0.75$; - - -, $1 - \bar{S} = 0.9$). In (d) and (e), thick curves denote results accounting for diffusion, and thin curves denote results neglecting diffusion.

and requiring $\delta < 2 \times 10^{-3}$ at $\gamma = 1$ and $\delta < 2 \times 10^{-5}$ at $\gamma = 10$ (see Figure 1). For $\gamma = 10$ and $\delta = 10^{-3}$, the distributions of instantaneous rates in Figure 4b show that, following an initial transient, photoinitiation propagates through the layer like a traveling wave. The results are nearly identical to those for the diffusionless ($\delta = 0$) case shown in Figure 3e of ref 1. One notable difference compared to the diffusionless case is the appearance of a local minimum (see Figure 4b) in the instantaneous profile of the initiation rate (near $z = 0.013$ when 10% of the initiator has been consumed).[27] This is a direct consequence of photoinitiator diffusion to the optical entrance at $z = 0$, leading to a higher photoinitiation rate there than predicted by the diffusionless model of ref 1. At larger values of δ, diffusion modifies the local photoinitiation rate profiles in two ways, both of which tend to diminish the traveling-wave character of the process. First, for $\delta = 0.01$ (see the Supporting Information), the initial transient is longer than for smaller δ. Second, for $\delta = 0.01$, the instantaneous initiation rate has a shallow minimum (near $z = 0.08$) when 25% of the initiator has been consumed. Finally, for the same δ, the maximum initiation rate at each fractional consumption of initiator is less localized than for smaller δ. Also, as found for $\delta = 10^{-3}$ at a smaller fractional consumption of initiator, the instan-

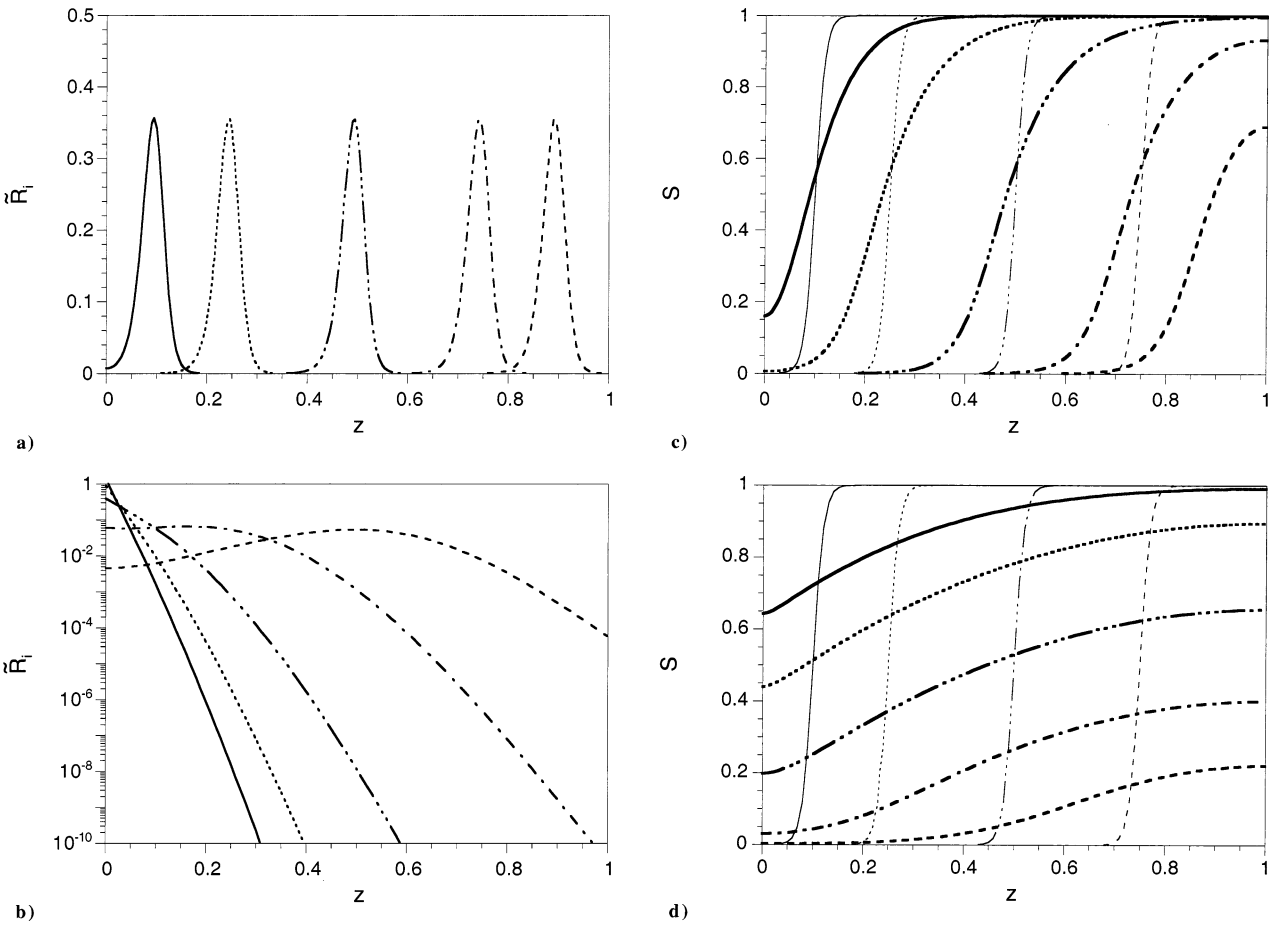

Figure 5. For $\gamma = 100$, (a) instantaneous initiation rate profiles for $\delta = 10^{-4}$, (b) instantaneous initiation rate profiles for $\delta = 0.01$, (c) instantaneous initiator concentration profiles for $\delta = 10^{-3}$, and (d) initiator concentration profiles for $\delta = 0.01$, all as functions of overall consumption of initiator (—, $1 - \bar{S} = 0.1$; ···, $1 - \bar{S} = 0.25$; —···—, $1 - \bar{S} = 0.5$; —·—, $1 - \bar{S} = 0.75$; - - -, $1 - \bar{S} = 0.9$). In (c) and (d), thick curves denote results accounting for diffusion, and thin curves denote results neglecting diffusion.

taneous initiation rate has a shallow local minimum (near $z = 0.15$) when 10% of the initiator has been consumed. As δ increases further, the process ultimately loses its traveling-wave character, as shown in Figure 4c for $\delta = 1$. In this case, diffusion is fast enough to maintain nearly uniform concentration, with the instantaneous rate profiles being nearly exponential in z, given by $\tilde{R}_i = 2\exp(-\gamma\bar{S}z)$ in the $\delta = \infty$ limit.

The concentration profiles for $\gamma = 10$ show a smooth transition from traveling-wave behavior at small δ to nearly uniform profiles at each degree of initiator consumption at high δ. For $\delta = 10^{-3}$, the concentration profiles (see the Supporting Information) are nearly identical to those for the diffusionless case (ref 1), except near the front and back walls. For $\delta = 0.01$, Figure 4d shows that diffusion has important effects, and that although the profiles still retain some of the character of a traveling wave, diffusion strongly affects the waveform at each stage of consumption. For $\delta = 0.1$, Figure 4e shows that the profiles are much more uniform, and that the traveling-wave behavior is only barely discernible. For $\delta = 1$, the profiles (see the Supporting Information) are nearly uniform, consistent with the dominant effect of diffusion.

***γ* = 100.** For $\gamma = 100$, Figure 1 shows that the variation of $\Delta\Theta$ with δ has an inflection point, unlike the results for smaller δ. At this large initial absorbance, the traveling-wave front in the diffusionless case is very thin, with $\tilde{R}_i$ having a half-width at half-maximum of $1.763/\gamma = 0.01763$ (see ref 1), and the half-width of the concentration profile being on the order of 0.02 (0.029 according to half the width of $z_{0.95} - z_{0.05}$ at $\bar{S} = 0.5$, and estimated at $0.02 = 0.5/(\partial\bar{S}/\partial z)$ according to the slope, evaluated at $z = 0.5$ and $\bar{S} = 0.5$, where z_S denotes the value of z at which the concentration assumes the value S). Thus, for this large absorbance, highly nonuniform absorption gives rise to concentration profiles having a second, intrinsic length scale much smaller than the layer thickness. Consequently, a much smaller value of δ (and hence a smaller diffusion coefficient) will suffice to maintain the nearly uniform concentration profile required for $\Delta\Theta \approx \gamma$. As a result, the "high-δ" plateau region extends to significantly smaller values of δ for $\gamma = 100$ than for smaller initial absorbances. For $\gamma = 100$, the leading-order approximation (19) breaks down in an intermediate range of δ, but is still very accurate at sufficiently large and small values of δ. The initial absorbance $\gamma = 100$ is the only value considered for which this second length scale is apparent; even for $\gamma = 10$, the thickness of the propagating concentration profiles (twice the half-widths of 0.29 and 0.2, computed according to the 5% and slope criteria, respectively) is not significantly less than the layer thickness, as shown in Figure 4b,c.

For $\gamma = 100$, the instantaneous initiation rate profiles approach the diffusionless case shown in Figure 3f of ref 1 for δ less than the smallest value shown ($\delta = 10^{-4}$). For $\delta = 10^{-4}$, Figure 5a shows that the initiation rate profiles are broader than for $\delta = 0$ (with profiles for $\delta = 10^{-4}$ overlapping and those for $\delta = 0$ not overlapping,

as shown in Figure 3f of ref 1), and that, for each degree of consumption, the local maximum value of $\tilde{R}_i$ lies noticeably below the diffusionless value of 0.5. For $\delta = 10^{-3}$, the instantaneous initiation rate profiles (see the Supporting Information) are "smeared" even more by diffusion, and the maximum rates are further reduced. As δ increases still more, Figure 5b (for $\delta = 0.01$) shows that diffusion has eliminated the traveling-wave character, while for $\delta = 1$, the profiles (see the Supporting Information) are essentially exponential in z, corresponding to $\tilde{R}_i = 2\exp(-\gamma\tilde{S}z)$.

For $\delta = 10^{-4}$, the shapes of the instantaneous concentration profiles (see the Supporting Information) are very nearly invariant, and simply translate downbeam as initiator is consumed. The profiles are nearly identical to those absent diffusion, with the presence of the front and back walls being felt only when the concentration gradient is large near a boundary, i.e., near the beginning and end of the process. Figure 5c ($\delta = 10^{-3}$) shows that, as δ increases, the profiles become less sharp and the effects of the boundaries are felt over a wider range of initiator consumption, although the traveling-wave nature of the process is still evident. As δ increases still further (see Figure 5d for $\delta = 0.01$ and the Supporting Information for $\delta = 1$), the traveling-wave character is ultimately lost. Finally, we note that the profiles at $\delta = 1$ are noticeably more uniform than the profiles at the same δ for $\gamma = 10$, even though the higher absorbance leads to greater nonuniformity in the diffusionless case. This is consistent with the discussion of a second length scale above, and shows that, for sufficiently large γ, a given value of δ (corresponding to a fixed diffusion coefficient) gives rise to more uniform concentration profiles as γ increases.

Discussion

The results presented in the previous section clearly show that, for a broad class of systems, diffusion leads to nonuniformity in the time-integrated primary radical production. This effect has its origin in the fact that diffusion replenishes initiator in the zone where it is most depleted, i.e., where initiator consumption is fastest. On the other hand, absent diffusion, each initiator molecule absorbs light and produces primary radicals at its initial location, giving rise to uniform time-integrated production of primary radicals.

Interpretation of the results in dimensional form requires only a simple transformation of dimensionless variables to dimensional ones. The front-to-back variation in the dimensional time-integrated primary radical production can be written as

$$\int_0^\infty [R_i(0,t) - R_i(L,t)]\,\mathrm{d}t = C_{A,0}\int_0^\infty [\tilde{R}_i(0,\tau) - \tilde{R}_i(1,\tau)]\,\mathrm{d}\tau = C_{A,0}\Delta\Theta \quad (20)$$

so that interpretation of the results in Figure 1 requires only multiplication by the initial initiator concentration to get the difference in radicals produced on a molar basis.

The results in Figure 1 show that, for a given layer (i.e., of fixed thickness, with fixed photoinitiator absorptivity and initial concentration), the degree of nonuniformity in time-integrated primary radical formation is a strong function of incident light intensity, I_o. The degree of nonuniformity varies from almost none at very high I_o (low δ) to a maximum value of $\gamma C_{A,0} = \alpha_A C_{A,0}^2 L$ at very low intensities (high δ), corresponding to the dependence on the period of time over which initiator is consumed, and over which diffusion has an opportunity to contribute to nonuniformity.

Whether diffusion-induced nonuniformity is desirable or undesirable depends on the application. When the objective is to produce a polymeric material in which the degree of monomer conversion and the molecular-weight (or chain-length) distribution are spatially uniform, nonuniformity in the overall (time-integrated) primary radical production will be generally undesirable. On the other hand, if the objective is to produce a layer with a graded variation of, say, permeability or diffusivity, then diffusion-induced nonuniformity offers a potentially attractive route. Reference to these two situations is made below.

Diffusion-Induced Nonuniformity in Previous Experiments. Significant diffusion-induced nonuniformity of the time-integrated primary radical production is likely to have occurred in several previous experimental studies of free-radical photopolymerization involving photobleaching initiators. An example is the frequently cited work of Tryson and Shultz,[28] who studied the kinetics of benzoin ethyl ether (BEE)-initiated photopolymerization of three acrylates using differential scanning calorimetry. For their initial BEE concentration of 1% (~0.04 M) and a BEE extinction coefficient of 780 M^{-1} cm^{-1},[3] we find that the initial absorbances lay in the range $2.23 \le \gamma \le 9.05$ for the four layer thicknesses used in the experiments. Using the highest intensity (attenuation of 0.044 mcal cm^{-2} s^{-1} by 60% using a neutral-density filter) and taking the quantum yield to be unity, we find (for $D = 10^{-5}$ cm^2 s^{-1}) that δ ranges from 0.64 for the thickest layer to 10.6 for the thinnest. Figure 1 shows that, for the smallest initial absorbance (corresponding to the 0.31 mm layer thickness), $\delta = 10.6$ is clearly on the high-δ asymptote, so that $\Delta\Theta \approx \gamma = 2.23$. For the highest initial absorbance (L = 1.26 mm, γ = 9.05), the high-δ asymptote extends to smaller δ, and we see that $\delta = 0.64$ will also give a value of $\Delta\Theta$ very close to γ. (Note that quantum yields less than unity serve only to increase δ, and that, for lower incident light intensities, corresponding to attenuation up to 96.9% by neutral-density filters in the experiments of Tryson and Shultz, δ will also be larger. In either case, the effect is to move $\Delta\Theta$ closer to its asymptotic value.)

In the experiments of Tryson and Shultz, in which no spatially resolved measurements were made, it is thus clear that diffusion should have led to considerable nonuniformity in the time-integrated primary radical production. Approximating $\Delta\Theta$ by γ, our analysis provides a lower bound for the front-to back ratio of time-integrated initiator photolysis rates $\Theta(0;\delta,\gamma)/\Theta(1;\delta,\gamma)$ of $\gamma/2 + 1$, where the denominator of the first term is the layer-averaged value of Θ, which bounds $\Theta(1;\delta,\gamma)$ from above. For $\gamma = 9.05$, this gives $\Theta(0;\delta,\gamma)/\Theta(1;\delta,\gamma) > 5.5$, meaning that more than 5 times as much initiator was photolyzed at the front of the layer than at the back. (In fact, the crude bound $\gamma/2 + 1$ greatly underestimates the nonuniformity. The actual front-to-back ratio given by (16) and (17) on the high-δ plateau is about 26.) Our analysis shows thus that, even for fairly thin layers, significant kinetic nonuniformity can occur.

Effects on Monomer Conversion and Chain-Length Distributions. Diffusion-induced nonuniformity of the time-integrated primary radical production

can have important consequences for photopolymerization, and can lead to significant errors in process models that do not account for initiator diffusion. The following discussion is confined to the case of high γ, for which the effects are most important.

Since diffusion reduces the instantaneous initiation rate in the back of the layer compared to the diffusion-free case, polymerization in the back will occur at lower radical concentrations, and with fewer overall primary radicals to initiate chains than would be predicted absent diffusion. The consequences of this depend on the initial absorbance γ and the ratio of diffusive and reactive time scales δ, as well as on two additional dimensionless parameters,[2,3] namely, the initial ratio of monomer and initiator concentrations and a kinetic parameter $\beta = k_p[fC_{A,0}/(\phi\alpha_A I_o k_t)]^{1/2}$, where k_p and k_t are the propagation and termination rate constants and f is the number of primary radicals produced per photoinitiator molecule consumed. The parameter β is equal to the first-order rate constant for monomer conversion divided by the first-order rate constant for initiator consumption, both evaluated at $z = \tau = 0$.

First, the diffusion-free analysis[2] predicts a strong dependence of conversion on β. For β less than about 1, the analysis predicts incomplete conversion of monomer, with less monomer converted at the front of the layer than at the back. This is a result of the fact that the highest primary radical concentrations (and hence highest termination rates) occur at the front of the layer. For small β, this leads to more recombination of primary and short-chain radicals at the front than at the back, and hence less monomer conversion near the front. The effect becomes stronger as γ increases. If δ is sufficiently large, initiator will diffuse upbeam to the propagating front of the traveling wave as initiator is consumed. We expect that this will lead to decreased conversion throughout the layer, since initiator that would otherwise have been photolyzed in its initial position will be photolyzed upbeam, at radical concentrations higher than would have obtained absent diffusion. For larger β, the diffusion-free analysis predicts that essentially all monomer will be converted. In this case, we expect that initiator diffusion will affect the degree of conversion only for a range of β (near unity) for which β is just sufficient to give complete conversion absent diffusion. In this case, we expect the effect to increase with increasing δ, and to vanish as $\delta \rightarrow 0$.

Diffusion-induced nonuniformity of time-integrated primary radical production can also be expected to affect the CLD and molecular-weight distribution. In our earlier diffusion-free analysis,[3] we found that, for large γ and small β, the CLD in the back of the layer is independent of z, and that the CLD shifts to shorter chain lengths upbeam. This is clearly a consequence of the fact that, at large γ, the initiator profiles resemble snapshots of a propagating wave, in which the initiator concentration changes in a small range of z, from almost completely consumed upbeam to nearly unreacted downbeam. At small β, monomer conversion near the optical entrance occurs under conditions of higher radical concentrations, with the consequence that termination rates are higher and the CLD is shifted to smaller chain lengths relative to the situation downbeam. When γ and β are both large, considerable monomer conversion occurs before arrival of the propagating front, under conditions where radical concentrations and termination rates are both low. At sufficiently high β, there is no depth beyond which the CLD becomes invariant with z, and in fact the CLD becomes increasing spatially nonuniform as β increases. This reflects the fact that the lowest radical concentrations (and hence the lowest termination rates) are maintained for the longest time at the back of the layer.

The effects of initiator diffusion will be manifested through changes in the shape of the propagating initiation wave. For large γ, diffusion will have the effect of "smearing out" the instantaneous initiation rate profiles, and reducing the maximum radical concentrations. When β is small, this should lead to longer chain lengths, with no significant effect on uniformity in the z-invariant region. When β is large, we expect that diffusion will lead to increased spatial variation of the CLD, since diffusion will reduce even further radical concentrations (and termination rates) throughout the layer. This would appear to have an effect similar to that of everywhere reducing the termination rate, which is equivalent to increasing β and hence the degree of spatial nonuniformity.[3]

Application to the Design of Functionally Graded Materials. Functionally graded polymeric materials, in which a deliberate spatially controlled variation of the CLD or degree of cross-linking is built into the material, have been proposed for use in controlled-release drug delivery applications.[29−31] Typical approaches to fabrication of such materials are multistep processes in which a number of discrete layers are polymerized under slightly different conditions.[30] These fabrication processes are complex, and the degree of nonuniformity achievable is typically *limited* by diffusion of monomer, initiator, or inhibitor. On the other hand, use of diffusion-induced nonuniformity offers a route to single-step fabrication of functionally graded polymeric materials, with no internal interlayer interfaces, and with a continuous variation of properties. The strength of the gradient should be controllable by the light intensity, a quantity that is in most cases easily adjustable over several orders of magnitude. The degree of monomer conversion or CLD nonuniformity achievable in any particular system can be predicted by using the initiator profiles presented above in models of monomer consumption and polymerization kinetics.

Limitations of the Model. Beyond those limitations of the model identified in our earlier work on the diffusion-free case[1] is the assumption that the diffusion coefficient of the photoinitiator is uniform and independent of the progress of reaction. In systems where significant polymerization occurs, one can expect D to decrease with increasing monomer conversion, to an extent that at each position and time depends on the local instantaneous chain-length distribution.[3] The effect of such diminution of the diffusion coefficient will be to alter the extent of the diffusion-induced nonuniformity. We believe that, in most cases, reduction of D as reaction progresses will have the effect of reducing the overall front-to-back nonuniformity $\Delta\Theta$ of the time-integrated primary radical production, with the magnitude of the effect depending on the spatial variation of the chain-length distribution.

Conclusion

For photobleaching initiators, the results presented show that significant nonuniformity in time-integrated primary radical production can be expected when layers with significant initial absorbance are photopolymer-

ized. The degree of nonuniformity is seen to depend on both the initial absorbance and a second dimensionless parameter, which is essentially the ratio of the rate of diffusion to the rate of initiator consumption. When diffusion is fast, initiator diffusion to the optical front of the layer can lead to significantly more initiator photolysis there than at the back, with the differences in overall radical production scaling quadratically with the initiator concentration. The results show that, in systems where homogeneity of the overall (e.g., time-integrated) production of primary radicals is important, the effects of diffusion must be minimized, by ensuring that photolysis is essentially completed before the effects of diffusion can be felt, for instance by increasing the light intensity. We also show that, for a given allowable degree of nonuniformity in the overall radical production, the tolerable value of the incident intensity increases as the initial absorbance increases.

General trends in the effects on monomer conversion and chain-length distributions are delineated.

Acknowledgment. Los Alamos National Laboratory is operated by the University of California for the U.S. Department of Energy under Contract W-7405-ENG-36.

Supporting Information Available: Figures showing the dependence of instantaneous concentration profiles and initiation rate profiles on extent of initiator consumption. This material is available free of charge via the Internet at http://pubs.acs.org.

References and Notes

(1) Terrones, G.; Pearlstein, A. J. *Macromolecules* **2001**, *34*, 3195−3204.
(2) Terrones, G.; Pearlstein, A. J. *Macromolecules* **2001**, *34*, 8894−8906.
(3) Terrones, G.; Pearlstein, A. J. *Macromolecules* **2003**, *36*, 6346−6358.
(4) Hutchinson, R. A.; Beuermann, S.; Paquet, D. A.; McMinn, J. H.; Jackson, C. *Macromolecules* **1998**, *31*, 1542−1547.
(5) Flach, L.; Chartoff, R. P. *Polym. Eng. Sci.* **1995**, *35*, 483−492.
(6) Flach, L.; Chartoff, R. P. *Polym. Eng. Sci.* **1995**, *35*, 493−498.
(7) Schaeffer, P.; Bertsch, A.; Corbel, S. Jézéquel, J. Y.; André, J. C. *J. Photochem. Photobiol.* **1997**, *107*, 283−290.
(8) Kodama, H. *Rev. Sci. Instrum.* **1981**, *52*, 1770−1773.
(9) Brulle, Y.; Bouchy, A.; Valance, B.; André, J. C. *J. Photochem. Photobiol.* **1994**, *83*, 29−37.
(10) Maffezzoli, A.; Terzi, R. *Thermochim. Acta* **1998**, *321*, 111−121.
(11) Flach, L.; Chartoff, R. P. *Polym. Eng. Sci.* **1995**, *35*, 483−492.
(12) Flach, L.; Chartoff, R. P. *Polym. Eng. Sci.* **1995**, *35*, 493−498.
(13) Hill-West, J. L.; Chowdhury, S. M.; Slepian, M. J.; Hubbell, J. A. *Proc. Natl. Acad. Sci. U.S.A.* **1994**, *91*, 5967−5971.
(14) Shultz, A. R.; Joshi, M. G. *J. Polym. Sci., Polym. Phys. Ed.* **1984**, *22*, 1753−1771.
(15) Krongauz, V. V. Diffusion in Polymer Matrix and Anisotropic Photopolymerization. In *Processes in Photoreactive Polymers*; Krongauz, V. V., Trifunac, A. D., Eds.; Chapman and Hall: New York, 1995.
(16) Hill, F. B.; Reiss, N.; Shendalman, L. H. *AIChE J.* **1968**, *14*, 798−804.
(17) Hill, F. B.; Reiss, N. *Can. J. Chem. Eng.* **1968**, *46*, 124−131.
(18) Shendalman, L. H.; Hill, F. B. *Chem. Eng. Sci.* **1969**, *24*, 909−911.
(19) Harano, Y.; Smith, J. M. *AIChE J.* **1968**, *14*, 584−591.
(20) Terrones, G.; Pearlstein, A. J. *J. Am. Chem. Soc.* **1991**, *113*, 2132−2140.
(21) Goodner, M. D.; Bowman, C. N. *Chem. Eng. Sci.* **2002**, *57*, 887−900.
(22) Miller, G. A.; Gou, L.; Narayanan, V.; Scranton, A. B. *J. Polym. Sci., Part A: Polym. Chem.* **2002**, *40*, 793−808.
(23) Encinas, M. V.; Majmud, C.; Garrido, J.; Lissi, E. A. *Macromolecules* **1989**, *22*, 563−566.
(24) Encinas, M. V.; Rufs, A. M.; Norambuena, E.; Giannotti, C. *J. Polym. Sci., A* **1997**, *35*, 3095−3100.
(25) Wegscheider, R. *Z. Phys. Chem.* **1923**, *103*, 273−306.
(26) Mitchell, A. R.; Griffiths, D. F. *The Finite Difference Method in Partial Differential Equations*; Wiley: New York, 1980.
(27) That the $\gamma = 10$ local minima shown for $\delta = 10^{-3}$ (Figure 4b) and $\delta = 0.01$ (Supporting Information) result from initiator diffusion to the front wall is seen as follows. When $\delta \neq 0$, the no-flux boundary conditions (7b) and (7c) require that the concentration profile must have extrema at $z = 0$ and 1. The former condition thus requires the concentration profile near $z = 0$ to be a local quadratic in z, as shown for each δ in Figure 4d,e and the Supporting Information. It is easy to show that the extremum at $z = 0$ must be a minimum. Thus, for sufficiently large γ, exponential attenuation of light on the nearly constant part of the concentration profile (near $z = 0$) leads to a decrease in the instantaneous initiation rate as z increases. Farther from the wall, however, where concentration increases quadratically with z, the postexponential factor in the second term on the right-hand side of (6) can lead to an *increase* in the instantaneous rate. The point is easily illustrated by approximating the concentration profile by $a + bz^2$, and substituting into the second term on the right-hand side of (6). One can easily show that if $27b > 64a^3\gamma^2$, then the local rate will have two extrema for $z > 0$, corresponding to the maximum and minimum we have computed.
(28) Tryson, G. R.; Shultz, A. R. *J. Polym. Sci. Polym. Phys. Ed.* **1979**, *17*, 2059−2075.
(29) Chang, R. K. *J. Pharm. Sci.* **1986**, *75*, 717−718.
(30) Lu, S.; Anseth, K. S. *J. Controlled Release* **1999**, *57*, 291−300.
(31) Georgiadis, M. C.; Kostoglou, M. *J. Controlled Release* **2001**, *77*, 273−285.

MA030451E